FEBS Letters 531 (2002) 314–318 FEBS 26694

NMR structure of the unliganded *Bombyx mori* pheromone-binding protein at physiological pH

Donghan Lee[a], Fred F. Damberger[a], Guihong Peng[b], Reto Horst[a], Peter Güntert[a,1], Larisa Nikonova[b], Walter S. Leal[b,c], Kurt Wüthrich[a,*]

[a] *Institut für Molekularbiologie und Biophysik, Eidgenössische Technische Hochschule-Zürich, CH-8093 Zürich, Switzerland*
[b] *National Institute of Agrobiological Science, Ibaraki 305-8634, Japan*
[c] *Department of Entomology, University of California, Davis, CA 95616, USA*

Received 31 July 2002; revised 20 September 2002; accepted 23 September 2002

First published online 15 October 2002

Edited by Thomas L. James

Abstract The nuclear magnetic resonance structure of the unliganded pheromone-binding protein (PBP) from *Bombyx mori* at pH above 6.5, BmPBP^{B}, consists of seven helices with residues 3–8, 16–22, 29–32, 46–59, 70–79, 84–100, and 107–124, and contains the three disulfide bridges 19–54, 50–108, and 97–117. This polypeptide fold encloses a large hydrophobic cavity, with a sufficient volume to accommodate the natural ligand bombykol. The polypeptide folds in free BmPBP^{B} and in crystals of a BmPBP–bombykol complex are nearly identical, indicating that the B-form of BmPBP in solution represents the active conformation for ligand binding.

Key words: Insect odorant-binding protein; *Bombyx mori* pheromone-binding protein; Hydrophobic cavity; pH-dependent conformational change; Nuclear magnetic resonance structure

1. Introduction

Females of the silkworm moth *Bombyx mori* produce a linear, partially unsaturated 16-carbon alcohol (bombykol [1]) as a sex pheromone that is recognized by the male at long distances and with high specificity. In the sensory organs of the male *B. mori*, bombykol is transported through the sensillar lymph to the olfactory receptors by a pheromone-binding protein, BmPBP, which occurs at high concentrations in moth olfactory hairs [2]. The crystal structure of BmPBP complexed with bombykol shows that the ligand is completely enclosed in the core of the protein [3]. This structure leaves open by which mechanism the ligand enters and exits BmPBP. Nuclear magnetic resonance (NMR) and circular dichroism spectroscopic investigations have shown that BmPBP exists in two different conformational states, depending on the pH [4,5]. NMR structure determination of the 'acidic form', BmPBP^{A}, present at pH 4.5, revealed a striking novel conformation when compared with the BmPBP–bombykol complex. This includes insertion of a helix formed by the C-terminal dodecapeptide into the space occupied by the ligand in the complex, the unraveling of the N-terminal helix of BmPBP in the complex, and significant changes in a loop covering the binding site [6]. The BmPBP^{A} structure thus provides a straightforward rationale for the observation that PBPs do not bind ligands below pH 5.0 [7,8]. To obtain a more complete picture of the mode of action of BmPBP, we have now determined the NMR structure of the unliganded form present at the physiological pH in the bulk sensillar lymph, i.e. pH 6.5, which we name BmPBP^{B}. BmPBP^{B} contains a hydrophobic cavity with sufficient volume to accommodate a bombykol molecule, indicating that it is the active conformation for pheromone binding.

2. Materials and methods

The expression and purification of ^{13}C,^{15}N-labeled BmPBP in *Escherichia coli* has been described previously [4]. The NMR sample used for the structure determination of BmPBP^{B} was prepared by dissolving 7 mg of lyophilized, uniformly ^{13}C,^{15}N-labeled BmPBP in 0.6 ml of 95% H_2O/5% D_2O containing 50 mM potassium phosphate buffer at pH 6.5 and 2 mM NaN_3, resulting in approximately 0.7 mM protein concentration. A biosynthetically directed 10% ^{13}C-labeled sample [9] was prepared in the same way, except that only 10% of the glucose supplied in the medium as the sole carbon source was uniformly ^{13}C-labeled.

2.1. NMR spectroscopy

All NMR measurements were performed at 20°C either on a Bruker DRX 500 spectrometer equipped with a cryogenic probe head, or on Bruker DRX 600 and DRX 750 spectrometers. All these instruments are equipped with four channels, and with triple resonance probe heads with shielded *z*-gradient coils. Proton chemical shifts are referenced to internal 2,2-dimethyl-2-silapentane-5-sulfonate, sodium salt (DSS). ^{13}C and ^{15}N chemical shifts are referenced indirectly to DSS, using absolute frequency ratios with the ^{1}H signals [10]. The spectra were processed with the program PROSA [11], and the program XEASY was used for the spectral analysis [12].

2.2. Structure determination and analysis

Peak lists of the three nuclear Overhauser effect spectroscopy (NOESY) spectra in Table 1 were generated as input for the programs CANDID and DYANA with the program XEASY [12] and automatic integration of the peak volumes with the program SPSCAN (Ralf Glaser, personal communication). The input further contained the chemical shift list corresponding to the sequence-specific assignments. NOE cross-peak assignments were then obtained with the pro-

*Corresponding author. Fax: (41)-1-633 1151.
E-mail address: kw@mol.biol.ethz.ch (K. Wüthrich).

[1] Present address: RIKEN Genomic Sciences Center, W505, 1-7-22 Suehiro, Tsurumi, Yokohama 230-0045, Japan.

Abbreviations: BmPBP, *Bombyx mori* pheromone-binding protein; BmPBP^{A}, the A-form of BmPBP; BmPBP^{B}, the B-form of BmPBP; DSS, 2,2-dimethyl-2-silapentane-5-sulfonate, sodium salt; NMR, nuclear magnetic resonance; NOE, nuclear Overhauser effect; NOESY, NOE spectroscopy; rmsd, root mean square deviation

0014-5793/02/$22.00 © 2002 Published by Elsevier Science B.V. on behalf of the Federation of European Biochemical Societies.
PII: S0014-5793(02)03548-2

gram CANDID [13] used in conjunction with three-dimensional structure calculations with the program DYANA [14]. The CANDID/DYANA calculation consisted of the standard protocol of seven cycles of iterative NOE assignment and structure calculation [13]. During the first six CANDID cycles, ambiguous distance constraints [15] were used, whereas for the final calculation only distance constraints corresponding to unambiguously assigned NOEs were retained. In each cycle, the DYANA input of NOE distance constraints assigned by CANDID was supplemented by 276 constraints for the backbone dihedral angles ϕ and ψ that were derived from $^{13}C^{\alpha}$ chemical shifts [16], 172 χ^1 and χ^2 side chain dihedral angle constraints derived from analysis of intraresidual NOE intensities [17], and the standard upper and lower distance constraints for the three disulfide bonds [18]. The 20 conformers with the lowest final DYANA target function values were energy-minimized in a water shell with the program OPALp [19,20], using the AMBER force field [21] (Table 2).

The program MOLMOL [22] was used to analyze the resulting 20 energy-minimized conformers and to prepare drawings of the structures. Secondary structure boundaries were defined using the algorithm of Kabsch and Sander [23], as implemented in MOLMOL. Internal cavities were characterized using the program VOIDOO [24].

3. Results

3.1. Resonance assignments and NMR structure determination of $BmPBP^B$

Sequence-specific assignments for the ^1H, ^{15}N and ^{13}C resonances of $BmPBP^B$ were obtained using standard 3D triple-resonance experiments, 3D ^{15}N- and ^{13}C-resolved [^1H,^1H]-NOESY spectra, and additional experiments for side chain assignments (Table 1). The backbone assignments are complete, with the exception of the amide groups of residues Gln 2, Tyr 34, Met 131 and Asp 132, the N-terminal amino group, C^{α} of Gln 2, and the carbonyl carbons of Ser 1, Ser 9, Phe 33, Ser 130 and Met 131. The amino acid side chain assignments of non-labile hydrogens are complete except for $C^{\delta}H_2$ and $C^{\varepsilon}H_2$ of Lys 6, Lys 14, and Lys 78, $C^{\delta}H_2$ of Lys 124, $C^{\gamma}H$ of Leu 10 and Leu 90, $C^{\varepsilon}H_3$ of Met 23 and Met 74, $C^{\beta}H_2$ and $C^{\varepsilon}H_3$ of Met 131, $C^{\beta}H_2$ and $C^{\gamma}H_2$ of Pro 129, $C^{\varepsilon 3}H$ and $C^{\zeta 3}H$ of Trp 37, and $C^{\varepsilon 1}H$ of His 80 and His 95. The labile side chain protons of Asn, Gln, Trp and Arg are completely assigned, with the sole exception of $N^{\delta}H_2$ of Asn 35. The absence of some H^N, ^{15}N and ^{13}C resonances in the loop of residues 33–46 and in the peptide segment of residues 129–132 is probably due to slow conformational exchange. The observation of strong sequential $d_{\alpha\delta}$ NOEs indicates that the prolyl residues 64, 102 and 129 are all in the *trans* conformation [25].

The peak lists derived interactively with the program XEASY [12] from the 3D ^{15}N- and ^{13}C-resolved [^1H,^1H]-NOESY spectra contained the chemical shift positions and the integrals for a total of 4685 cross-peaks, which includes numerous redundancies as well as NOEs corresponding to covalent structure-fixed distances. Together with a list of the ^1H, ^{15}N, and ^{13}C chemical shifts derived from the sequence-specific assignments, this provided the input for the programs CANDID [13] and DYANA [14], which yielded assignments for 2041 'meaningful' NOE upper distance limits and the NMR structure of $BmPBP^B$ with the statistics given in Table 2 (for details, see Section 2). The global rmsd values relative to the mean coordinates of 0.95 Å calculated for the backbone heavy atoms of residues 1–128 and 1.39 Å for all heavy atoms of the same polypeptide segment show that the precision of the structure determination is significantly lower than for $BmPBP^A$ [6].

3.2. The NMR structure of $BmPBP^B$

The solution structure of $BmPBP^B$ is composed of seven α-helices arranged into a globular domain of residues 1–128, and an 'unstructured' tail of residues 129–142 (Fig. 2). The seven helices span the residues 3–8 (α1a), 16–22 (α1b), 29–32 (α2), 46–59 (α3), 70–79 (α4), 84–100 (α5), and 107–124 (α6) (Fig. 1), where the notation α1a and α1b corresponds to

Table 1
Survey of the NMR experiments used to obtain sequence-specific resonance assignments and the conformational constraints for the $BmPBP^B$ structure determination

Spectrum[a]	ν_0 (^1H) (MHz)	Nuclei[b]	Data size[b] (complex points)	t_{1max}, t_{2max}, t_{3max} [b] (ms)
Backbone assignments				
2D [^{15}N,^1H]-COSY	500	^{15}N, ^1H	307×1024	128, 122
3D HNCA	600	^{15}N, ^{13}C, ^1H	34×30×1024	21.5, 7.5, 136.4
3D HNCACB	600	^{15}N, ^{13}C, ^1H	34×64×1024	19.6, 7.3, 122.9
3D CBCA(CO)NH	600	^{15}N, ^{13}C, ^1H	34×10×1024	19.6, 1.14, 129.9
3D TROSY-HNCO	500	^{15}N, ^{13}C, ^1H	32×32×1024	10, 9.6, 136.4
Aliphatic side chain assignments[c]				
2D [^{13}C,^1H]-COSY[d]	600	^{13}C, ^1H	800×1024	44.2, 73.1
2D ct-[^{13}C,^1H]-COSY	600	^{13}C, ^1H	256×1024	21.3, 122
3D ^{15}N-resolved [^1H,^1H]-TOCSY	600	^{15}N, ^1H, ^1H	34×150×512	18.4, 18, 64.9
3D H(C)CH-COSY	750	^{13}C, ^1H, ^1H	35×150×1024	19.6, 7.3, 122.9
3D H(C)CH-TOCSY	600	^{13}C, ^1H, ^1H	55×140×512	10.1, 16.8, 61.4
3D (H)CCH-COSY	500	^{13}C, ^{13}C, ^1H	46×66×1024	20.7, 29.7, 85.2
Aromatic side chain assignments[e]				
2D [^{13}C,^1H]-TROSY	600	^{13}C, ^1H	75×1024	13.2, 285
3D TROSY-(H)CCH-COSY	600	^{13}C, ^{13}C, ^1H	32×58×1024	6.4, 11.6, 102.4
Conformational constraints				
3D ^{15}N-resolved [^1H,^1H]-NOESY	750	^{15}N, ^1H, ^1H	28×150×1024	16.1, 18, 129.9
3D ^{13}C-resolved [^1H,^1H]-NOESY[c]	750	^{13}C, ^1H, ^1H	28×150×1024	6.6, 22.2, 113.9
3D ^{13}C-resolved [^1H,^1H]-NOESY[e]	750	^{13}C, ^1H, ^1H	32×290×1024	6.8, 30.8, 108.9

[a]Unless otherwise indicated, a sample of uniformly ^{13}C,^{15}N-labeled BmPBP in 0.6 ml of 95% H_2O/5% D_2O containing 50 mM potassium phosphate buffer was used to measure the spectra, which were all obtained at 20°C.
[b]The dimensions were collected such that the final entry is the acquisition dimension.
[c]The ^{13}C carrier frequency was placed in the center of the aliphatic region at 35 ppm.
[d]Measured using 10% biosynthetically directed ^{13}C-labeled BmPBP [9].
[e]The ^{13}C carrier frequency was placed in the center of the aromatic region at 125 ppm.

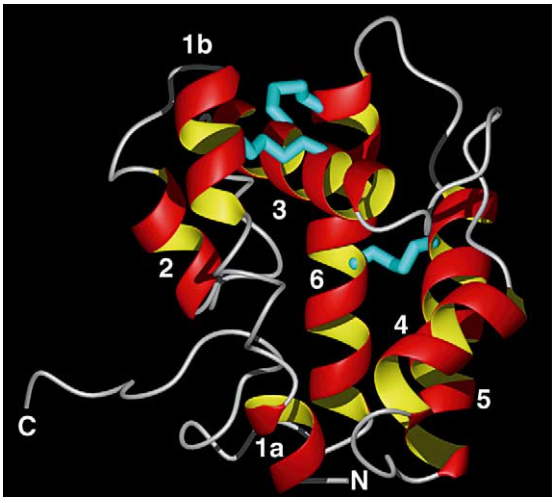

Fig. 1. Ribbon drawing of one of the 20 energy-minimized DYANA conformers of BmPBP^B. The N- and C-termini are indicated. The α-helices are colored red and yellow, and labeled with the numbers specified in Table 2. Polypeptide segments with non-regular secondary structure are drawn as a gray line. The three disulfide bridges are shown in cyan. This and all other figures were prepared with the program MOLMOL [22].

nomenclature introduced in previous structural studies of alternative conformational states of BmPBP [3,6]. The loops linking the helices are named after the helix preceding them, so that the loop following the helix α1a is L1a. The loops are well-defined, except for L2 with the 14 residues 33–45 (Fig. 2), where several resonances are missing, presumably due to conformational exchange. All six cysteinyl residues are involved in disulfide bridges, as verified by the fact that their C$^\beta$ chemical shifts are all equal to or larger than 35 ppm [10], and the framework of helices is stabilized by the three disulfide bridges Cys19–Cys54, connecting the helices α1b and α3, Cys50–Cys108 between α3 and α6, and Cys97–Cys117 between α5 and α6 (Fig. 1). The network of NOE distance constraints is consistent with the chemically determined disulfide bonds [26,27]. There are also a large number of non-covalent hydrophobic contacts between the side chains of the different helices. Each of the seven helices in BmPBP^B includes one or more C-capping interactions, and α5 and α6 also contain N-capping hydrogen bonds [28]. Except for L2, the loops connecting the helices contain numerous H-bonds; this helps to explain their well-ordered structures (Fig. 2).

To further characterize the apparent increased structural disorder in the C-terminal tail and the loop L2, we measured ^{15}N{^{1}H}-NOEs (data not shown). These show clearly that the tail of residues 129–142 is flexibly disordered, and that the loop L2 of residues 33–45 also shows increased mobility. For both of these polypeptide segments, medium-range ^{1}H–^{1}H NOEs are scarce and there are no long-range NOEs, which is compatible with a flexibly disordered conformation.

The most striking feature of the solution structure of BmPBP^B is a hydrophobic cavity with a volume of 272 ± 17 Å^3 (Fig. 3), which corresponds closely to the volume of bombykol (264 Å^3) [3]. This cavity corresponds to the space occupied by bombykol in the BmPBP–bombykol complex (Fig. 4). It is lined with the 21 hydrophobic side chains Met 5 and Leu 8 from the helix α1a, Phe 12 from the loop L1a, Phe 33, Tyr 34 and Phe 36 from L2, Ile 52 from α3, Met 61, Leu 62 and Leu 68 from L3, Ala 73, Phe 76 and Ala 77 from α4, Ala 87, Leu 90, Ile 91 and Val 94 from α5, and Trp 110, Val 114, Ala 115 and Phe 118 from α6. It also contains four polar side chains of Asp 32 from α2, Thr 48 and Ser 56 from α3, and

Table 2
Input for the calculation and characterization of the energy-minimized NMR structures of BmPBP^B

Quantity	Value[a]
NOE upper distance limits[b]	2041
Dihedral angle constraints (ϕ, ψ, χ^1 and χ^2)	448
Residual target function value (Å^2)	1.83 ± 0.45
Residual distance constraint violations	
Number ≥ 0.1 Å	20 ± 6
Maximum (Å)	0.14 ± 0.03
Residual dihedral angle constraint violations	
Number ≥ 2.5°	1 ± 1
Maximum (degrees)	2.48 ± 0.81
AMBER energies (kcal/mol)	
Total	−5326 ± 92
van der Waals	−401 ± 17
Electrostatic	−6030 ± 82
rmsd from ideal geometry	
Bond lengths (Å)	0.0074 ± 0.0001
Bond angles (degrees)	1.90 ± 0.05
rmsd to the mean coordinates (Å)	
N, C$^\alpha$, C′ (1–33, 43–128)	0.77 ± 0.16
All heavy atoms (1–33, 43–128)	1.13 ± 0.14
N, C$^\alpha$, C′ (1–128)	0.95 ± 0.16
All heavy atoms (1–128)	1.39 ± 0.14
N, C$^\alpha$, C′ of regular secondary structures[c]	0.62 ± 0.14
All heavy atoms of regular secondary structures[c]	1.04 ± 0.13

[a]Except for the top two entries, the data characterize the bundle of 20 conformers used to represent the NMR structure; the mean value and the standard deviation are given.
[b]The input also included the standard nine upper and nine lower distance constraints to enforce the three disulfide bonds 19–54, 50–108, and 97–117 [18,26,27].
[c]Regular secondary structure elements are the α-helices 1a (residues 3–8), 1b (16–22), 2 (29–32), 3 (46–59), 4 (70–79), 5 (84–100), and 6 (107–124).

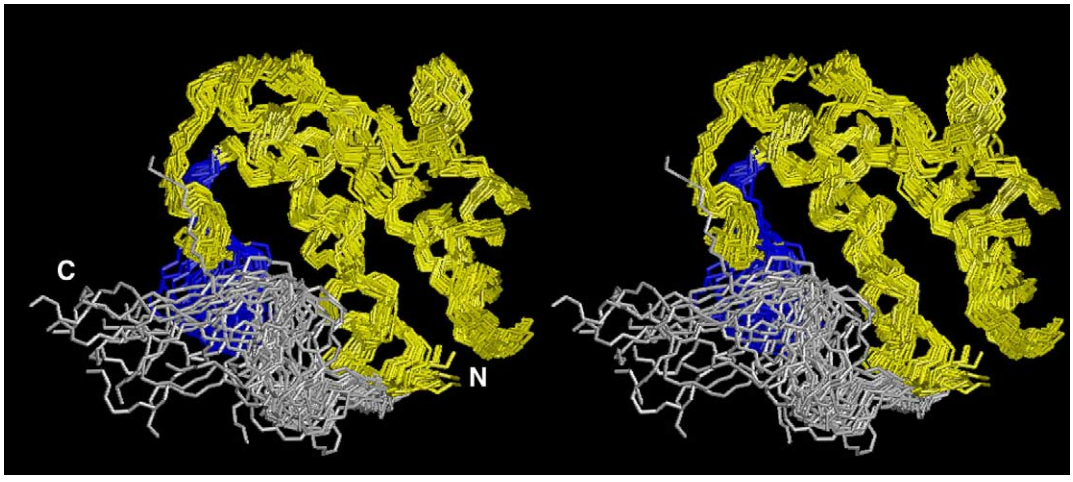

Fig. 2. Stereo view of a superposition for minimal rmsd of the backbone atoms in the residues 1–128 in 20 energy-minimized DYANA conformers representing the NMR structure of BmPBP^{B}. The poorly ordered loop of residues 33–45 is shown in blue, the unstructured C-terminal tail of residues 129–142 is gray, and all other residues are yellow.

Glu 98 from α5. A superposition for best fit of the heavy atoms of these side chains gives an rmsd of 1.2 Å, indicating that the positions of most of these side chains are well defined. Actually, if one excludes the residues Asp 32, Tyr 34 and Phe 36 from α2 and L2, one calculates a rmsd of 0.89 Å, which is comparable to the global backbone rmsd for the segment 1–128 (Table 2).

3.3. Data bank deposition

The atomic coordinates of the 20 energy-minimized DYANA conformers of BmPBP^{B} have been deposited at the RCSB Protein Data Bank (www.rcsb.org) under the PDB Accession code 1LS8.

4. Discussion

Comparison of the structure of BmPBP^{B} with that of the PBP polypeptide chain in the crystal structure of a BmPBP–bombykol complex [3] shows two nearly identical folds (Fig. 4), with an average backbone rmsd value of 1.00 Å calculated for N, C$^{\alpha}$ and C′ of the residues 1–128 between the ensemble of BmPBP^{B} conformers (Fig. 2) and the complex. Previously the framework of the helices α1b, α3, α5 and α6 was shown to be nearly invariant between BmPBP^{A} and the BmPBP–bombykol complex [4], and it is now found to be preserved also in BmPBP^{B}. Superposition of the backbone heavy atoms of residues 16–22 from α1b, 46–55 from α3, 84–100 from α5, and 107–122 from α6 results in an rmsd value of 0.62 Å between BmPBP^{A} and BmPBP^{B}, and 0.50 Å between the protein in the BmPBP–bombykol complex and BmPBP^{B}. This striking preservation of a structural scaffold of four helices among three structures that show pronounced conformational differences in other molecular regions can be rationalized at least in part through the anchoring of these four helices by three disulfide bonds (Fig. 1). The inherent rigidity of the

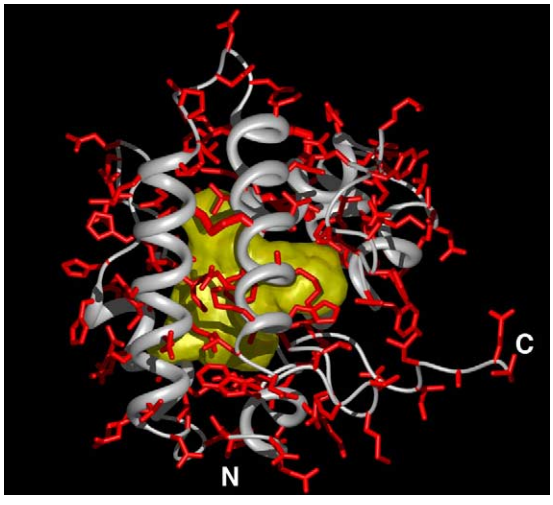

Fig. 3. All-heavy-atom presentation of the NMR structure of BmPBP^{B} illustrating the central cavity. The backbone is shown as a gray spline function through the C$^{\alpha}$ positions, and side chains are shown in red. The surface of the hydrophobic cavity is shown in yellow.

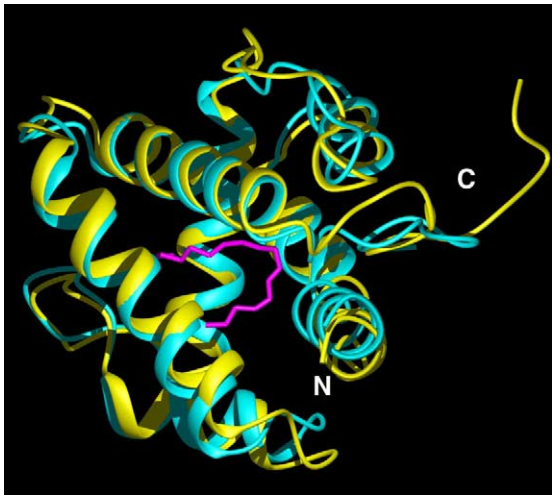

Fig. 4. Comparison of the NMR structure of unliganded BmPBP^{B} and the crystal structure of a BmPBP–bombykol complex [3]. Free BmPBP^{B} is shown in yellow. In the complex, the protein is cyan, and bombykol is magenta. The backbone atoms for residues 1–128 have been superimposed for best fit, with an rmsd value of 1.00 Å. The N- and C-termini are indicated.

disulfide-linked four-helix scaffold is probably also primarily responsible for the fact that a large-volume hydrophobic cavity is preserved in the absence of the ligand.

In some proteins, hydrophobic cavities serving as ligand-binding sites have been observed to collapse partially in the absence of a ligand that would support their structure [29–31]. In other proteins, corresponding hydrophobic cavities appear to be fully preserved also in the absence of the ligand [32,33]. This includes a member of the non-specific lipid transfer proteins found in plants [33] and the human serum albumin [32]. Both the plant proteins and human serum albumin show no significant sequence homology to PBPs, but they are also stabilized by inter-helix disulfide bridges, and similar to BmPBP these proteins are presumed to be involved in the transport of small hydrophobic ligands across a polar solvent environment [29–33]. $BmPBP^{B}$ thus appears to be an addition to a so far small collection of all-helical disulfide-rich transport proteins that maintain a full-size ligand-binding cavity in the unliganded state. One is intuitively led to the conclusion that this high-pH form of BmPBP is the reactive conformation, pre-shaped for ligand binding with only minimal conformation change. These considerations further provide a rationale for the observation that the low-pH form of BmPBP does not bind bombykol, since in $BmPBP^{A}$ the potential binding cavity is occupied by a helix formed by the C-terminal dodecapeptide segment, which is flexibly unstructured in $BmPBP^{B}$ (Fig. 2).

Acknowledgements: Financial support was obtained from the Schweizerischer Nationalfonds (Projects 31.49047.96 and 31.66427.01), a Bundesstipendium for D. Lee, the Japanese Program for Promotion of Basic Research Activities for Innovative Biosciences, and direct financial support from the Department, the College, and the Chancellor's office at the University of California-Davis.

References

[1] Hansson, B.S. (1995) Experientia 51, 1003–1027.
[2] Steinbrecht, R.A. (1998) Ann. NY Acad. Sci. 855, 323–332.
[3] Sandler, B.H., Nikonova, L., Leal, W.S. and Clardy, J. (2000) Chem. Biol. 7, 143–151.
[4] Damberger, F., Nikonova, L., Horst, R., Peng, G.H., Leal, W.S. and Wüthrich, K. (2000) Protein Sci. 9, 1038–1041.
[5] Wojtasek, H. and Leal, W.S. (1999) J. Biol. Chem. 274, 30950–30956.
[6] Horst, R., Damberger, F., Luginbühl, P., Güntert, P., Peng, G., Nikonova, L., Leal, W.S. and Wüthrich, K. (2001) Proc. Natl. Acad. Sci. USA 98, 14374–14379.
[7] Prestwich, G.D. (1993) Protein Sci. 2, 420–428.
[8] Briand, L., Nespoulous, C., Huet, J.C., Takahashi, M. and Pernollet, J.C. (2001) Eur. J. Biochem. 268, 752–760.
[9] Senn, H., Werner, B., Messerle, B.A., Weber, C., Traber, R. and Wüthrich, K. (1989) FEBS Lett. 249, 113–118.
[10] Wishart, D.S., Bigam, C.G., Yao, J., Abildgard, F., Dyson, H.J., Oldfield, E., Markley, J.L. and Sykes, B.D. (1995) J. Biomol. NMR 6, 135–140.
[11] Güntert, P., Dötsch, V., Wider, G. and Wüthrich, K. (1992) J. Biomol. NMR 2, 619–629.
[12] Bartels, C., Xia, T.H., Billeter, M., Güntert, P. and Wüthrich, K. (1995) J. Biomol. NMR 6, 1–10.
[13] Herrmann, T., Güntert, P. and Wüthrich, K. (2002) J. Mol. Biol. 319, 209–227.
[14] Güntert, P., Mumenthaler, C. and Wüthrich, K. (1997) J. Mol. Biol. 273, 283–298.
[15] Nilges, M., Macias, M.J., Odonoghue, S.I. and Oschkinat, H. (1997) J. Mol. Biol. 269, 408–422.
[16] Luginbühl, P., Szyperski, T. and Wüthrich, K. (1995) J. Magn. Reson. B 109, 229–233.
[17] Güntert, P., Billeter, M., Ohlenschläger, O., Brown, L.R. and Wüthrich, K. (1998) J. Biomol. NMR 12, 543–548.
[18] Williamson, M.P., Havel, T.F. and Wüthrich, K. (1985) J. Mol. Biol. 182, 295–315.
[19] Luginbühl, P., Güntert, P., Billeter, M. and Wüthrich, K. (1996) J. Biomol. NMR 8, 136–146.
[20] Koradi, R., Billeter, M. and Güntert, P. (2000) Comput. Phys. Commun. 124, 139–147.
[21] Cornell, W.D., Cieplak, P., Bayly, C.I., Gould, I.R., Merz, K.M., Ferguson, D.M., Spellmeyer, D.C., Fox, T., Caldwell, J.W. and Kollman, P.A. (1996) J. Am. Chem. Soc. 118, 2309–2309.
[22] Koradi, R., Billeter, M. and Wüthrich, K. (1996) J. Mol. Graph. 14, 51–55.
[23] Kabsch, W. and Sander, C. (1983) Biopolymers 22, 2577–2637.
[24] Kleywegt, G.J. and Jones, T.A. (1994) Acta Crystallogr. D 50, 178–185.
[25] Wüthrich, K. (1986) NMR of Proteins and Nucleic Acids, Wiley, New York.
[26] Leal, W.S., Nikonova, L. and Peng, G.H. (1999) FEBS Lett. 464, 85–90.
[27] Scaloni, A., Monti, M., Angeli, S. and Pelosi, P. (1999) Biochem. Biophys. Res. Commun. 266, 386–391.
[28] Aurora, R. and Rose, G.D. (1998) Protein Sci. 7, 21–38.
[29] Charvolin, D., Douliez, J.P., Marion, D., Cohen-Addad, C. and Pebay-Peyroula, E. (1999) Eur. J. Biochem. 264, 562–568.
[30] Han, G.W., Lee, J.Y., Song, H.K., Chang, C.S., Min, K., Moon, J., Shin, D.H., Kopka, M.L., Sawaya, M.R., Yuan, H.S., Kim, T.D., Choe, J., Lim, D., Moon, H.J. and Suh, S.W. (2001) J. Mol. Biol. 308, 263–278.
[31] Lerche, M.H., Kragelund, B.B., Bech, L.M. and Poulsen, F.M. (1997) Structure 5, 291–306.
[32] Curry, S., Mandelkow, H., Brick, P. and Franks, N. (1998) Nature Struct. Biol. 5, 827–835.
[33] Shin, D.H., Lee, J.Y., Hwang, K.Y., Kim, K.K. and Suh, S.W. (1995) Structure 3, 189–199.